J. Phys. D: Appl. Phys. **33** (2000) 2133–2141. Printed in the UK PII: S0022-3727(00)12399-X

# A critical condition in Fresnel diffraction used for ultra-high resolution lithographic printing

**A J Bourdillon†, C B Boothroyd‡, J R Kong† and Y Vladimirsky†§**

† Singapore Synchrotron Light Source, National University of Singapore, 5 Research Link, Singapore 117603
‡ Department of Materials Science and Metallurgy, Pembroke Street, Cambridge, CB2 3QZ, UK

Received 8 March 2000

**Abstract.** The adoption of a novel method for producing fine features by 1 nm proximity x-ray lithography would solve all of the current technical limitations to its extensibility. These limitations include the fabrication of fine features on masks and the maintenance of narrow mask–wafer gaps. Previously, with demagnification by bias, we described line features of 43 nm width produced with comparatively large clear mask features and large mask–wafer gaps. The method is generally applicable and has been shown to be extensible to beyond 25 nm printed features sizes on the wafer. The demagnification, $\times 1$–$\times 6$, is a result of Fresnel diffraction and occurs without lenses or mirrors. The method takes advantage of the modern control of resist processing and has good exposure stability. We now expand on the optimization of the process by defining and explaining the critical condition and by demonstrating the consistency of various types of simulation. The simulations demonstrate the effects of the gap width, non-symmetric rectangular masks, spectral bandwidth, outriggers, T junctions, blur, etc. In two-dimensional images, the spectral bandwidth allows sharp features due to interference and effectively eliminates ripple parallel to the longer dimension. Demagnification by exposure near the critical condition extends the most mature of the next generation lithographies which we define generically—following actual current lithographic practice—in terms of the departure from the classical requirement for fidelity in the reproduction of masks. Specifically, for 1 nm proximity lithography, demagnification of critical features greatly facilitates the printing of fine features.

## 1. Introduction

In a previous rapid communication [1] we outlined an entirely novel approach to proximity x-ray lithography involving our definition of next generation lithography (NGL) as the departure from the classical requirement for fidelity in the reproduction of masks‖. In particular we drop the prior requirement that 1 nm proximity x-ray lithography should be 1:1. We demagnified clear mask features in the image produced on the wafer by the positive use of Fresnel diffraction and combined this with the modern control in resist processing. A reduction of $\times 1$–$\times 6$, from comparatively large mask apertures, was obtained. Without either lenses or mirrors, the demagnification occurs with comparatively large mask–wafer gaps, short exposure times and high stability in the exposures. A demagnification of $\times 3.5$ for printed features of 43 nm was demonstrated using a mask–wafer gap of 30 $\mu$m. With this fundamental solution to all the critical issues described in the prior art [2], we showed that the demagnification, which occurs by the positive and deliberate use of bias, provides extensibility for 1 nm proximity x-ray lithography to beyond 25 nm. In this paper we expand on the theory and features of the process which were too detailed to include in the previous rapid communication.

Among NGLs competing for the sub-100 nm patterning, 1 nm proximity x-ray lithography [3] is the most advanced and mature [2, 4–6]. Many functional devices have been developed [7], in several laboratories, by the use of proximity x-ray lithography for critical levels. Commercial toolsets and masks are readily available. Typically, a mask pattern, fabricated by electron beam writing, is copied by proximity printing of x-rays, in the energy band of 1–2 keV, through a small gap onto a silicon wafer that is being processed. Typically synchrotron radiation is used and this is naturally

§ Present address: JMAR Research, 3956 Sorento Valley Boulevard, San Diego, CA 9212, USA.

‖ Classical lithography is based on the concept of fidelity in reproducing the mask pattern onto the wafer. The impending crisis in lithography results from inescapable limits associated with this fidelity. Shrinking critical dimension requirements in semiconductor manufacturing demand the development of lithographic techniques producing the desired patterns that are not necessarily replicas of the mask patterns. Some illustrations are phase shifters, outriggers, serifs and auxiliary features in optical lithography, interferometric lithography and strutted and stencil mask in electron- and ion-beam projection lithographies. NGL implies, and is here defined as, the *departure from the classical concept of replication fidelity*. NGL replaces the more narrow term—post optical lithography.

0022-3727/00/172133+09$30.00  

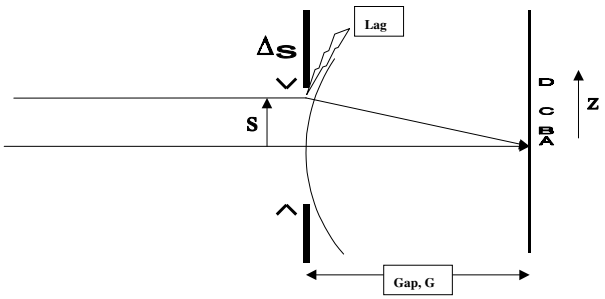


**Figure 1.** Two rays of light from a distant synchroron source passing through a slit of width $\Delta s$ (corresponding to a clear transmitting mask feature) and constructing an image (see figure 2 below) at the axial point $A$ on the plane of the wafer. The upper ray suffers a phase lag proportional to $s^2/\lambda$.

collimated by relativity so that the penumbra is controlled to within about 1 nm (cf point sources [5]). To provide uniform illumination, the x-ray beam is typically scanned, by an oscillating mirror, across the mask and wafer system. Exposures of full fields, typically $30 \times 30$ mm$^2$, are made in a time of about 1 s, the dose being in the range tens of millijoules per square centimetre and dependent on the precise optics used. The mask is held stationary while the wafer is stepped and aligned between exposures on different fields.

## 2. Fresnel diffraction

### 2.1. Fresnel diffraction in one dimension

Optical image formation in proximity printing is described by Fresnel diffraction [4]. In x-ray lithography an additional important factor is the photoelectron blur, and the resulting aerial image is a convolution of these functions [5]. The relation between feature size $\omega$, wavelength $\lambda$ and distance $G$ from the object to the 'image' plane, where the shadow of the feature is cast, can be formulated in terms of the number of Fresnel (half-wavelength) zones. Reliable imaging requires at least two Fresnel zones, and the 'resolution' or minimum feature size $W$ is usually expressed as

$$W = k\sqrt{\lambda G} \tag{1}$$

with $k = \sqrt{2}$ as a 'diffraction limit' value [4]. The actual feature size reproduced in a lithographic process also depends on the resist and process, plus several other factors, which can all be reduced generally to a coefficient. The diffraction phenomenon is a deterministic process, well predictable, and, in proper circumstances, highly reproducible. The realization of lithographic imaging far below the 'diffraction limit' is facilitated by optimizing the exposure to a desirable level of intensity. Examples of x-ray lithographic printing of features down to 16 nm ($k \sim 0.65$) in positive resists are reported elsewhere [5, 8]. A further decrease of the $k$ value ($k \sim 0.54$–0.60) was achieved using a so-called 'low-dose' exposure technique of a high-contrast positive resist [9] (see table 1 of [1]). Consider first the imaging of uni-dimensional (1D) lines before progressing to two-dimensional (2D) imaging of rectangular apertures, etc.

Diffraction is associated with redirecting part of the light from open areas into a geometrical shadow under an opaque feature [10]. Most of this diffracted light comes from the illuminated area adjacent to the edge of the feature, producing a shift of the edge image away from its geometrical position. Thus, the printed feature size is 'biased' compared with that on the mask. Even the image of a straight edge is shifted compared with the geometrical shadow. This bias phenomenon can be illustrated and estimated by analysing the well known Fresnel diffraction due to a straight edge [1, 9]. Figure 1 shows rays from a distant source interfering at a point $A$ on the wafer, intersecting the plane through the centre of a slit and parallel to the incident beam. The various rays suffer phase lags which depend on $s^2/\lambda$. The vectorial addition of the amplitudes of rays passing through the slit is represented mathematically with the Fresnel integrals:

$$x = \int_0^v \cos\frac{\pi v^2}{2}\,\mathrm{d}v \tag{2}$$

and

$$y = \int \sin\frac{\pi v^2}{2}\,\mathrm{d}v \tag{3}$$

where the dimensionless spatial coordinate $v$ is related to the coordinate $s$ in the plane of the slit:

$$v = s\left(\frac{2}{G\lambda}\right)^{1/2} = (2\tilde{N}_F)^{1/2} \tag{4}$$

with $\tilde{N}_F$ the number of Fresnel zones; while on the image plane

$$v' = z\left(\frac{2}{G\lambda}\right)^{1/2}. \tag{5}$$

The Fresnel integrals can be represented graphically with Cornu's spiral, shown in figure 2, i.e. the vibration curve. Here the amplitudes and phases due to bunches of rays (as in figure 1) can be represented in the conventional way [9] by arrows lying along the spiral at corresponding values of $v$. The intensities are proportional to the square of vectorially summed amplitudes. As examples, at an image plane with gap $G$, the vectorial sum of the amplitudes transmitted by a slit are represented by vectors such as $A$, $B$, $C$ and $D$ in figure 2. $A$, being symmetric, is on the central plane of the slit where $z = 0$ (figure 1); while $B$, $C$ and $D$ have increasing $z$ as in figure 1. The last level lies opposite the slit edge corresponding to 1:1 mask:wafer imaging. Notice that, as drawn, $A$ is a maximum. This is because the gap is set for the critical condition† which we define as

$$\Delta v_{max} = 2.419 = \Delta s\left(\frac{2}{\lambda G}\right)^{1/2} \tag{6}$$

i.e. spanning the points on the Cornu spiral for which, at maximum, $\mathrm{d}y/\mathrm{d}x = -x/y$.

At this condition, the dose has a particular form consisting of a narrow head on two shoulders, as in figure 3. The explanation for the shoulders is easily seen in figure 2.

† The critical condition is critical only in certain respects, including the maximum at the wavevector $A$ (figure 2). The exposure stability is not so critical.

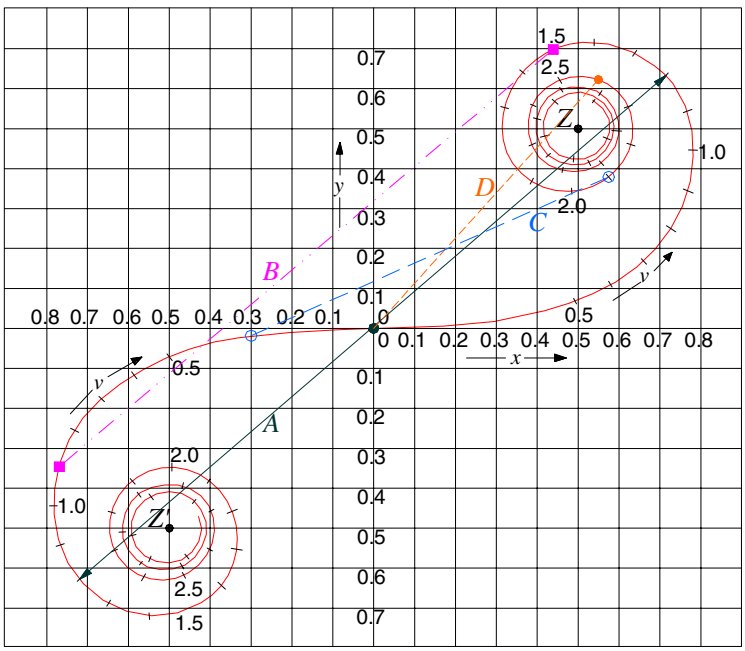


**Figure 2.** Cornu spiral showing vectors representing wave amplitudes in the Fresnel diffraction at points $A$, $B$, $C$ and $D$ (see figure 1) on the plane of the wafer. The amplitude of $A$ is the maximum since it represents the critical condition for which the slit width $\Delta s = 2.419(\lambda G/2)^{1/2}$. Scanning from the axis along the image plane in the direction of $z$ (figure 1) the amplitude decreases rapidly past $B$, forms a shoulder at $C$ and decreases rapidly again past $D$. The corresponding intensities are shown in figure 3.

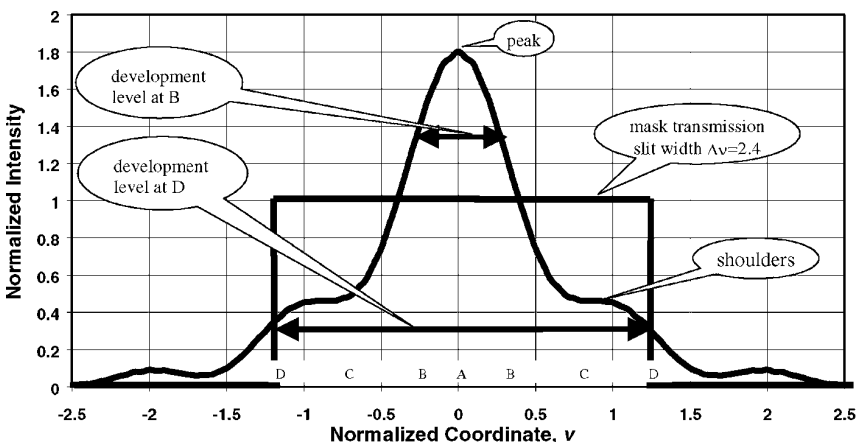


**Figure 3.** Aerial image of a slit at the critical condition showing a peak at $A$. Also shown are a $\times 4$ demagnified image of the slit at the development level $B$ and a 1:1 image at the development level $D$. The normalized coordinate $v = x(2/G\lambda)^{1/2}$ at the wafer and corresponds to $2.419 = \Delta s(2/G\lambda)^{1/2}$ at the mask, where transmission is shown.

As $\Delta v'$ is scanned, from the symmetric position $A$ along the Cornu spiral, the wavevector joining its ends becomes rapidly shorter at $B$, stays roughly constant at the shoulder $C$ and gets rapidly shorter again at $D$. Here it can be seen from figures 2 and 3 that the intensity level directly under the absorber edge, level $D$, is about 25% of the nominal intensity (with amplitude $ZZ'$). The 25% intensity level (with amplitude $\sim ZO$, to the origin) is valid for any wavelength and/or gap.

Depending on the development conditions, the printed feature edge can be formed at different levels of intensity relative to the nominal dose, and as a consequence the image of the edge is shifted, by corresponding amounts, into the illuminated (open) area of the mask feature. A line or a trench in the resist (formed by two edges of the absorber) will be respectively wider or narrower than those on the mask. To compensate for this, the opaque features on the mask can be 'positively' biased, which implies that the absorber has to be made narrower by a two-sided bias. Alternatively, by selecting a convenient development at a suitable point on the aerial image, for example level $B$ (figure 3) where the demagnification is $\times 4$, a demagnification of $\times 1$–$\times 6$ can generally be produced. Notice that by choosing a development level at a high dose, e.g. level $B$, the exposure time is effectively reduced, i.e. one-fifth of the time needed for level $D$.

The two-sided bias is the difference in length between the horizontal double arrows at levels $B$ and $D$ in figure 3. We

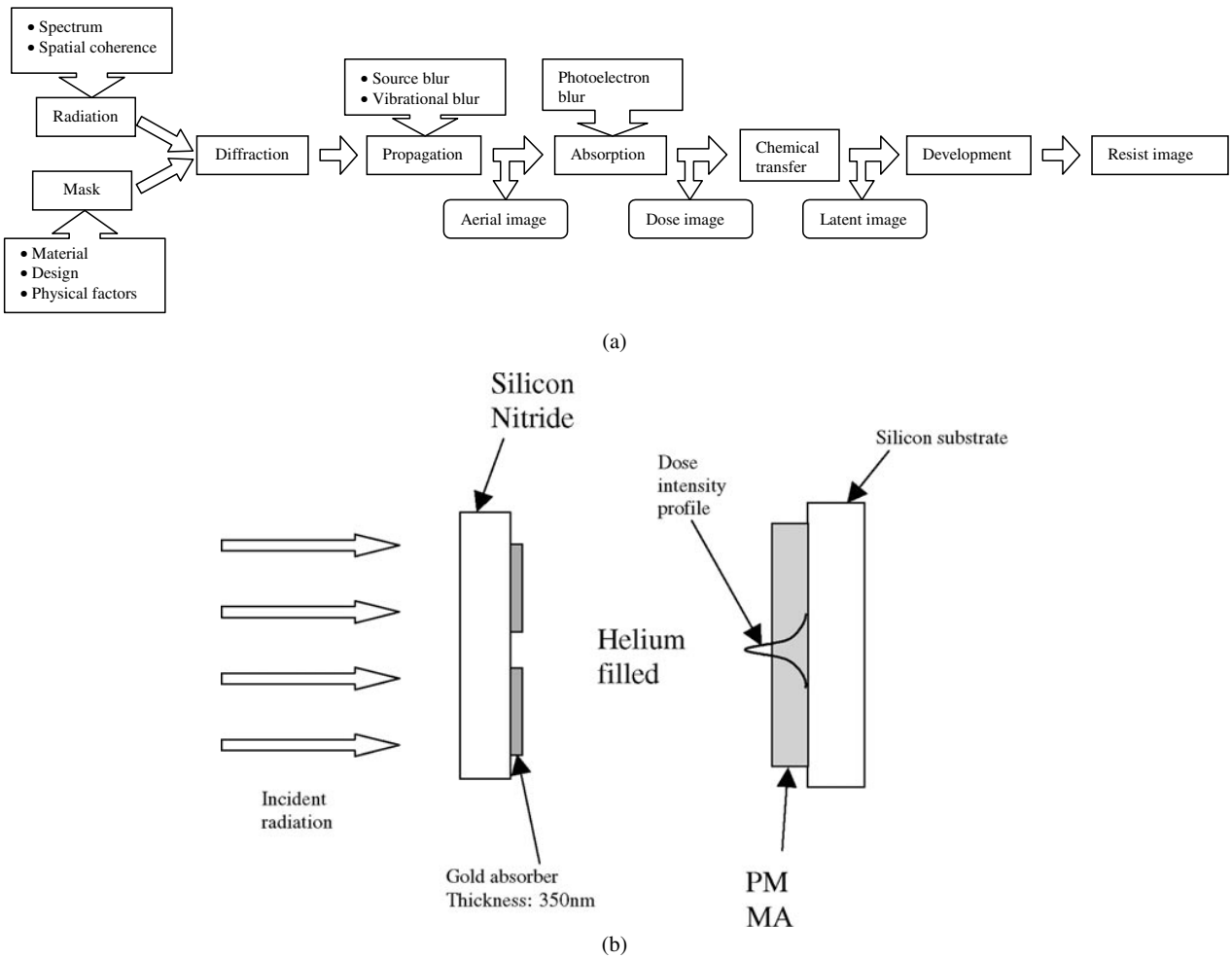


**Figure 4.** Schematic diagram of (a) the processes involved in the image formation using the Xstepper and (b) the arrangement of the elements involved in the simulation.

have previously shown [1] that with an appropriate resist and processing and with the positive use of this bias, $b$, the value for $k$ in equation (1) can be reduced from 1.4 to $k_\omega = 0.2$ for a printed feature size $\omega = W - b$. Then the demagnification by bias,

$$D_{emag} = \frac{W}{\omega} = \frac{k}{k_\omega} \tag{7}$$

providing practical demagnification between $\times 1$ and $\times 6$ depending on the development level, for example 0.35 at level $D$ (figure 3) and 1.35 at level $B$ for a demagnification of $\times 4$.

An analysis of diffraction image formation in resist (0.5 $\mu$m thick PMMA) was performed using the Xstepper Toolset [2, 9, 11] developed at the Center for Nanotechnology (CNTech) at the University of Wisconsin-Madison. This toolset uses the diffraction representation in the Sommerfeld approximation [12]. In these simulations, the latent resist images (absorbed dose distribution) were obtained using the parameters of the Aladdin synchrotron at CNTech's ES-5 (two mirror) beamline, with an x-ray mask having 2 $\mu$m thick carrier and 0.35 $\mu$m thick Au absorber. The parameter space used for imaging included: isolated clear features and equal line/space patterns ranging from 50 to 450 nm; from 5 to 30 $\mu$m mask–wafer gaps; incoherent blur in the range from 0 to 50 nm; and a realistic spectral bandwidth. The latent image profile width (representing development) was determined at different levels of absorbed dose, normalized to the incident intensity, and was plotted as a function of the linewidth of the mask feature.

Figure 4 is a flowchart showing the inputs to the Xstepper used in the simulation and the arrangement of the elements. The radiation propagates through a series of media (figure 4(b)) and the slice method [13] is used to calculate the transmission. This is a 'beam propagation' method [14, 15] used iteratively from layer to layer through space. The synchrotron radiation source is partially spatially coherent and was approximated by a blur function in the software. Additional sources of blur, for example due to stepper vibrations, can be included. At the point before the radiation interacts with the resist, an aerial image is formed at the wafer plane. This is the diffracted intensity due to the mask pattern and gives an indication of the imaging process. The output of the intensity is available at this point and subsequently, after absorption by the resist, where the dose image is calculated. After considering the transfer of energy into the chemical reaction, which results in either the scission or cross linking of the polymer chains within the resist, the latent image is formed. With the data of the resist modelled, an image of the developed resist can be

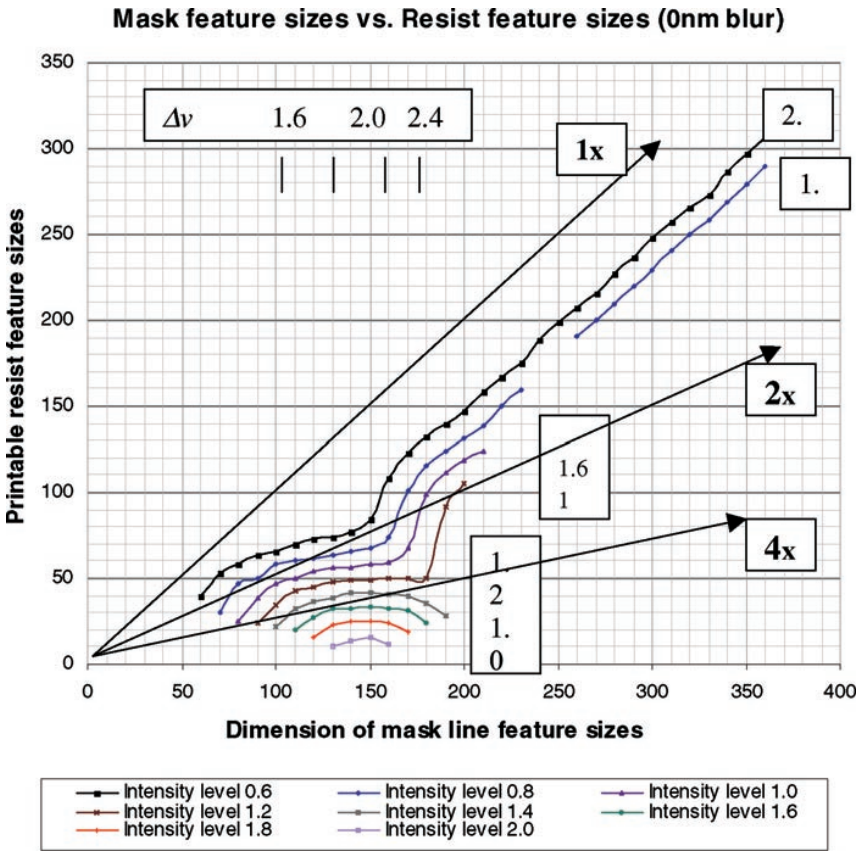


**Figure 5.** The printable resist feature size against the clear mask feature size at a 10 $\mu$m gap and various development levels, as shown, and no blur. The simulations were made for isolated lines using realistic incident bandwidth. Arrows show lines at $\times 1$, $\times 2$ and $\times 4$ magnification. The dimensionless slit width $\Delta v$ is also shown for corresponding mask feature sizes.

derived. This last resist-specific step was not implemented in the results reported here. Instead, the dose image is used for the derivation of the printable linewidth of features in the resist.

In figure 5, the results of a computer simulation are presented using the feature sizes formed in a resist at a 10 $\mu$m gap when developed to various levels of dose intensity. It can be seen that development to a level (see the ordinates in figure 3) between 1.6 and 1.8 will yield 20–30 nm features from a 150 nm clear feature on the mask, thus demonstrating demagnification of $\times 4$–$\times 6$. The arrows marked $1\times$, $2\times$ and $4\times$ correspond to the respective lines of demagnification. The curves representing simulation results tend to straight lines at the larger mask features, when the slope is close to that of the $1\times$ line. The shift along the ordinate axis then represents bias which is larger at higher intensity development levels. The region of smaller mask features ($<$200 nm) is of special interest. Three aspects are significant: (a) in this region higher degrees of demagnification can be achieved; (b) the feature size formed in the resist is only slightly dependent on the mask feature size, especially at higher demagnifications; and (c) the curves corresponding to various dose levels are positioned closer together here than in the other regions. These aspects translate to an enhanced linewidth control, a relaxed mask critical dimension (CD) requirement and a sufficiently wide dose latitude.

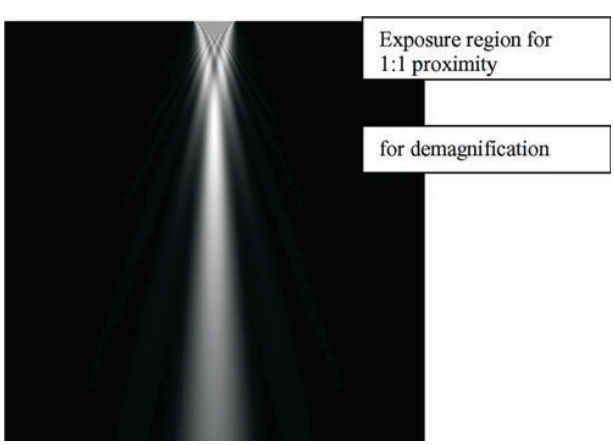


**Figure 6.** Simulation of a Fresnel diffracted current, with wavelength $\lambda = 0.8$ nm, passing through a slit of width 150 nm. The picture width is 1536 nm and the height 40 $\mu$m. The critical condition lies at a gap of 10 $\mu$m. Notice the sharp peak and adjacent shoulders as in figure 3.

Figure 5 is a good approximation for small blur and the exposure stability is illustrated by the range of values of $\Delta v$ for which selected mask feature sizes can be printed. Effects due to blur are specific to the resists used and have been examined elsewhere [16].

To understand the independent effects of the mask feature size, wavelength and gap on the 2D images, idealized

simulations were performed for the intensities below the mask. A routine was used which is based on the multislice method written in the Semper [17] image processing program. This routine allows the Fresnel diffraction from arbitrary masks in one and two dimensions to be calculated at any distance from the mask. The x-ray intensities up to 30 $\mu$m below a 150 nm wide mask illuminated with 0.8 nm wavelength x-rays are shown in figure 6. It can be seen that the critical condition for the narrowest and brightest line occurs at about 10 $\mu$m below the mask. At this depth a sharp peak adjacent to two shoulders is evident. Close to the mask the picture is different. The simulation demonstrates the inherent limitation in 1:1 proximity imaging while, by contrast, showing the broad latitude in exposure stability on demagnification near the critical condition. The dimensionless slit width $\Delta v$ may vary between values of 1.4–3.0 while preserving the consistent peak on shoulder (figure 3) shape used in the demagnification.

Figure 6 is a simulation for a mask having opaque absorbers. By comparison, the effect of partial transmission from the mask absorber is shown in figure 7. The transmission of the absorbers is then 32.4%, corresponding to the transmission through 450 nm of Ta at a wavelength of 0.8 nm. The absorption coefficient was taken from the *International Tables for Crystallography*. However the energy range of 1–2 keV includes the Ta M edge and so the transmission will, in the case of absorbers made of this material, vary over this range. The main differences between figures 6 and 7 can be seen in the profiles (figure 7(b)) taken across the images at 30 $\mu$m from the mask (three-quarters of the way from the top of the images). Although there is little difference in the height of the maxima, there is broadening in the latter case, shown by the thin line in figure 7(b). The smaller subsidiary fringes vary considerably with wavelength (here shown for 0.8 nm x-rays corresponding to a 1.5 kV photon energy) and so, with a 1–2 kV spectral bandwidth, will tend to average out. More important averages due to this bandwidth are shown in the following 2D simulations.

### 2.2. Fresnel diffraction in two dimensions

Figure 8(a) shows a rectangular aperture representing 150 × 600 nm$^2$, dimensions. In figure 8(b), the simulated image at a distance 30 $\mu$m behind the aperture is shown. Then $\Delta v = 1.3$. The image is demagnified, as expected, and some ripple is also found. This correlates qualitatively with the ripple classically observed at high spread in a dimensionless slit width [10], $\Delta v = \Delta s(2/G\lambda)^{1/2} = (2N_F)^{1/2}$, where $\Delta s$ represents the slit width (figure 1) in laboratory dimensions and $N_F$ represents the number of Fresnel half zones [1]. This type of ripple is familiar in the well known Fresnel diffraction pattern due to a knife edge. When the aperture is not symmetrical, as in figure 8(a), the critical condition cannot be maintained at the same time in both dimensions. The critical condition therefore refers to the finer dimension where high-resolution printing is most difficult to achieve. Close to the critical condition, as in figure 8(c) where the gap is 9.8 $\mu$m and $\Delta v = 2.4$, the ripple is reduced, its frequency increased and the image sharpened. In the latter two figures, the wavelength simulated is 0.8 nm. In practice

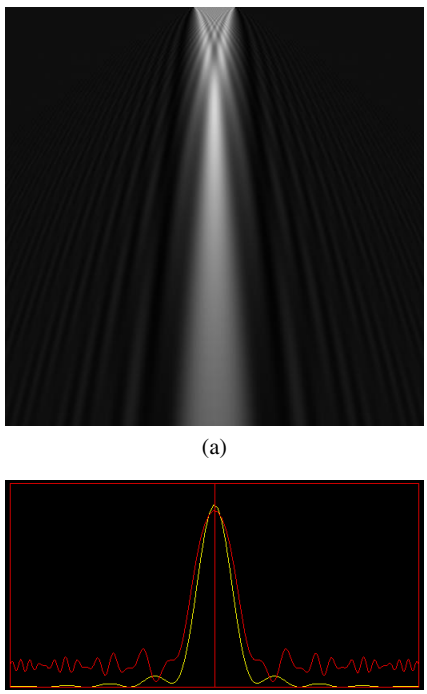

(a)

(b)

**Figure 7.** (a) Simulated image due to 32.4% transparency of tantalum mask absorber, 450 nm thick, for slit conditions as in figure 5 and (b) the effect of the transparency shown by cross sections from figures 6 (thick line) and 7(a) (thin line) at a distance 30 $\mu$m behind the mask. The maxima are the same, but the transparency causes line broadening.

this ripple is significantly reduced by the wide bandwidth in the incident beam, photoelectric blur, acid diffusion in the resists etc. A blur function of 10–20 nm may be considered as typical [1] and is used later in this paper. The effect of a flat bandwidth 0.62 nm $< \lambda <$ 1.28 nm is to significantly reduce the ripple. This is represented in figure 8(d) where mean $\Delta v$, $\langle \Delta v \rangle$, is 2.4, as in figure 8(c). *In particular, note that with a wide bandwidth while the ripple is effectively eliminated the resolution is preserved owing to interference of waves on either side of the mean*, i.e. the resolution and the demagnification are not, to the first order, affected. By contrast, the effect of changing the monochromatic wavelength is simply represented in the first order by changing $\Delta v$ [10]. An analysis of the simulations using estimates of the incident spectra [7], instead of the uniformly flat spectrum used in figure 8(d), will be included in future work.

At greater distances behind the mask, i.e. beyond the critical condition, the effective $\Delta v$ for the larger dimension is reduced, so that the ripple becomes more pronounced. The demagnification is also reduced. It is therefore advantageous to expose close to the critical condition.

The image can be squared off by the use of outriggers. This is demonstrated in the simulations shown in figure 9. It is clear that with further judicious application of inriggers, or with chopped corners, etc, the bright spots at the extremities of a rectangular image can also be reduced.

The ripple adopts higher frequencies at the T intersection, as shown in the simulation shown in figure 10(b).

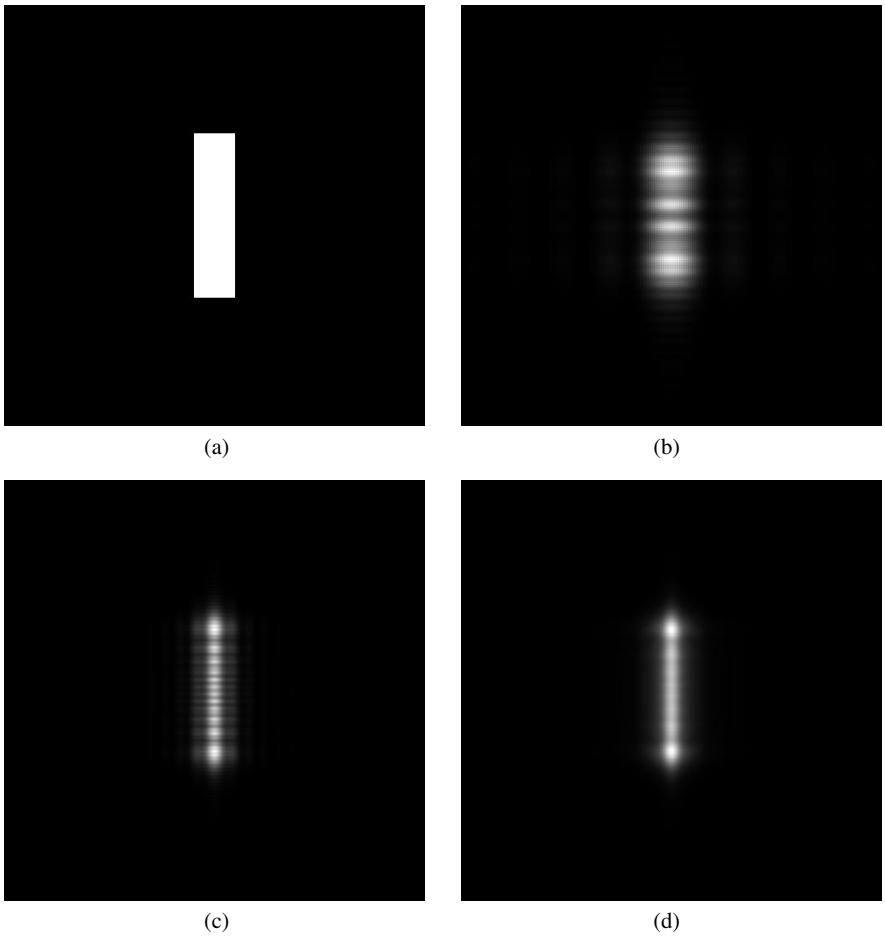


**Figure 8.** (a) 2D rectangular slit of size $150 \times 600$ nm$^2$; (b) simulated image due to 0.8 nm x-rays transmitted at a distance of 30 $\mu$m behind opaque mask and aperture in figure 7(a), when for the critical (narrower) width, $\Delta v = 1.4$; (c) simulated image due to 0.8 nm x-rays transmitted at a distance of 9.8 $\mu$m behind the opaque mask and aperture as in figure 7(a), with $\Delta v = 2.4$. Notice the ripple in the image intensity due to the longer dimension and bright fringes at the ends both significantly reduced in (d) simulated under the same conditions but using a flat band pass ranging over 0.62 nm $< \lambda <$ 1.28 nm and mean $\langle \Delta v \rangle = 2.7$. Notice that when the mean $\langle \Delta v \rangle$ differs from critical condition, the image reverts towards figure 7(b), resolution is lost and ripples are enhanced.

These high frequencies will be well averaged by a wide bandwidth and blur. However beyond the critical condition, as in figure 10(c), the image becomes more distorted with a shift in the brightness off the cross arm and towards the vertical leg.

## 3. Experimental results

A series of preliminary exposures were performed using a UV-6 deep UV resist at the CNTech ES-3 beamline equipped with a SAL 200/M x-ray stepper. The exposure and processing conditions were as follows: a 0.5 $\mu$m thick resist layer (using a post-applied bake at 130 °C for 60 s and post-exposure bake at 130 °C for 90 s) was exposed to a 200 mJ cm$^{-2}$ dose (450 mJ cm$^{-2}$ on the mask) with a mask–wafer gap of 20 $\mu$m and then developed in a standard LDD-26W Shipley developer for 45 s. The print shown in figure 11(a) was exposed to a grating mask with 300 nm wide clear features and a 600 nm period provides 107 nm wide lines at a demagnification of $\times$2.8. In figure 11(b) the print is due to a grating mask with 200 nm wide clear features and a 400 nm period at a $\times$2.4 demagnification. These prints are consistent with our earlier work [1] in which 43 nm wide lines were printed from 150 nm wide clear mask features.

## 4. Discussion and conclusion

When the features on a mask are compared with those on the wafer, the results can be interpreted in terms of the local 'demagnification'. This demagnification, although achieved without lenses or mirrors, offers the same advantage for CD control as the advantage of having larger features on a mask used in $\times$4-projection lithography. The extensibility limit depends on the photoelectric blur and on practical mask–wafer gaps. An experimental value for $k = 0.25$ has been used to demonstrate [1] extensibility beyond 25 nm with gaps of 5–10 $\mu$m.

There exists a critical condition at which the demagnified images are optimized with respect to resolution. The condition is a function of the clear mask feature size, wavelength and gap setting. The exposure stability is strong in the theoretical case of monochromatic incident radiation. When, as in practical arrangements, the x-rays are contained in a wide band of radiation, then, provided the means is

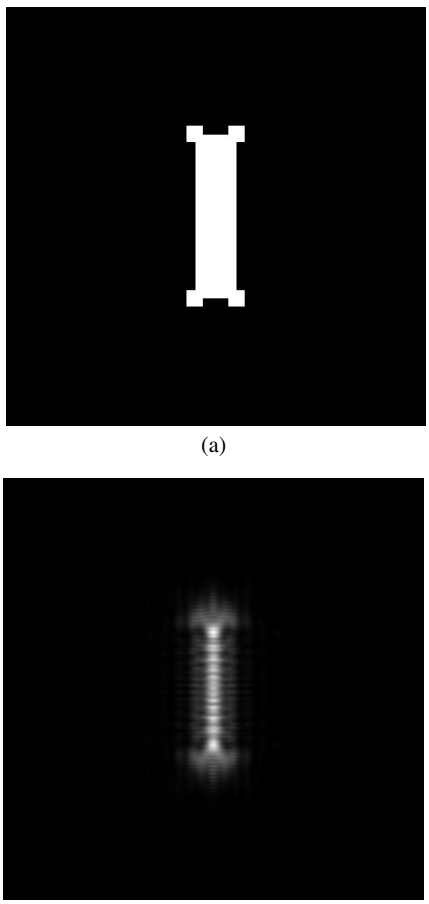

(a)

(b)

**Figure 9.** (a) Mask aperture, as in figure 8(a), but equipped with outriggers; (b) simulated image at a distance of 9.8 $\mu$m behind the opaque mask and aperture with the outriggers shown in (a). Compared with figure 8(c), the bright fringes at ends are now squared off.

close to the critical condition, there is an insignificant loss in resolution even though the dimensionless spatial coordinate, $v$, covers a range of values. This is a useful effect of interference. When the mean lies away from the critical condition, simulations show there is serious loss in resolution due to the wide bandwidth.

When the mask features are not symmetric in two dimensions, the critical condition cannot be maintained in both dimensions at the same time. Then this condition is taken to refer to the smaller dimension where the resolution is harder to achieve. The ripple is generated parallel to the larger dimension due to an increased dimensionless slit width $\Delta v$. This ripple is most obviously simulated for the case of monochromatic x-rays; but it is mostly eliminated when a typical band width is used in the exposures. This elimination of ripple is desirable and is optimized when the smaller dimension is at the critical condition.

Due to a large bias, fine features formed by proximity printing are isolated. To produce nested features, or dense lines, and to fulfill the 'DRAM half-pitch' imaging requirements in device fabrication, special techniques are being developed [1]. Using mask features with a large bias (50–150 nm), double or multiple exposures and, possibly,

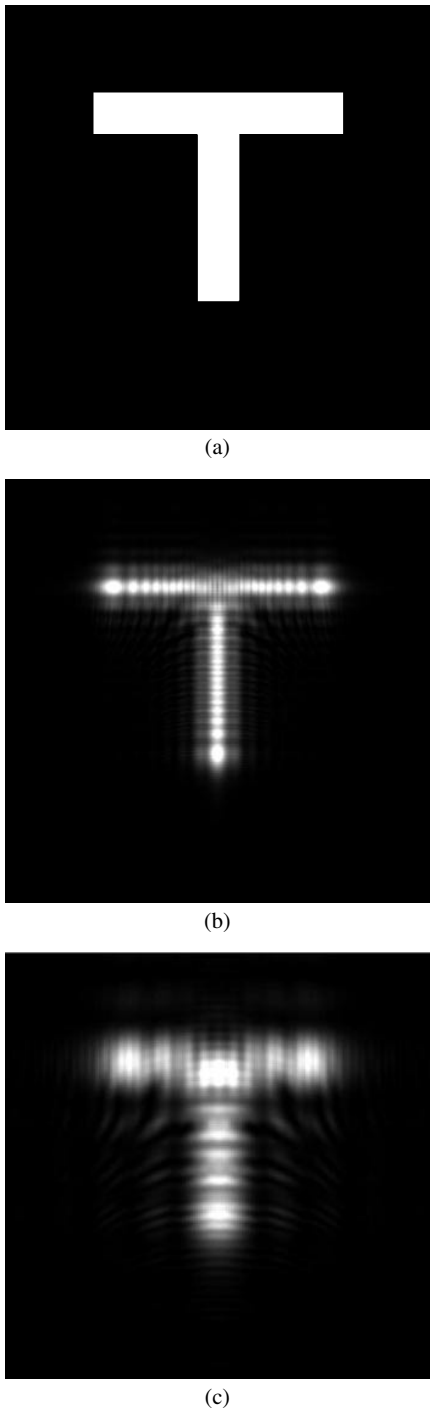

(a)

(b)

(c)

**Figure 10.** (a) T-shaped mask aperture with the vertical leg the same as figure 8(a) plus a horizontal arm 150 nm $\times$ 900 nm; (b) simulated image at a distance 9.8 $\mu$m behind the opaque mask and aperture shown in (a); (c) simulated image at distance 30 $\mu$m behind opaque mask and aperture shown in (a). These simulations are both made for monochromatic x-rays with $\lambda = 0.8$ nm. A wide incident bandwidth will smooth the ripple.

complementary masks can be used. For example, a triple exposure, followed by a single development step, can be performed by sequential relative mask–wafer shifts. The intensities of these three exposures are added incoherently. The dose delivered during each partial exposure is a fraction

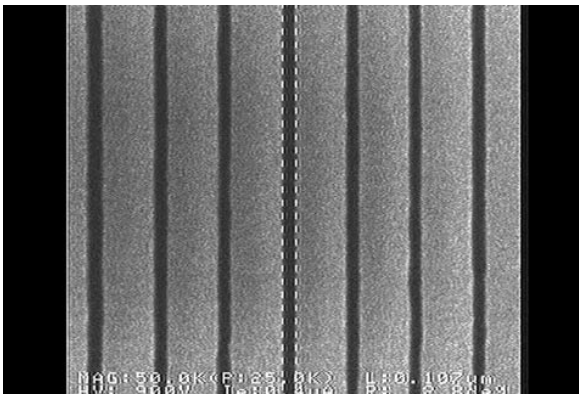

(a)

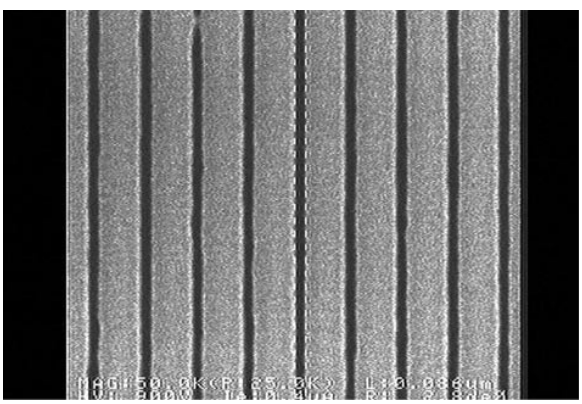

(b)

**Figure 11.** (a) 107 nm lines printed in the UV-6 positive resist from clear mask features of 300 nm width and a period of 600 nm and (b) 86 nm lines printed from clear mask features of 200 nm width and a 400 nm period.

($\sim\frac{1}{3}$–$\frac{1}{2}$) of the required dose, so the exposure time is close to that of a conventional single exposure. The techniques depend to some extent on the resist response and such responses are being evaluated, for the purpose, from a variety of resists.

On the basis of the 1D and 2D simulations and experimental results presented, the following conclusions can be drawn: (a) proximity lithography offers an effective local $\times 1$–$\times 6$ demagnification and associated advantages of relaxed mask CD requirements and extensibility beyond 25 nm; (b) the optimum condition for demagnification is shown to lie on the critical condition where $\Delta v = 2.419$; (c) even away from this condition, simulations show that the exposure stability is high and that the conventional broad band 1–2 kV x-rays can be used as in the prior art; (d) when clear mask features are not symmetric in two dimensions, non-uniformities in dose that are simulated for monochromatic x-rays are smoothed by beams with a wide band width. The smoothing occurs without significant losses in resolution in the finer dimension.

Finally, bias optimization can be used, as is shown here, to significantly enhance resolution. This is the case in proximity lithography in particular. We have considered that in projection lithographies, Fresnel fringes and resist processing might also be used, although to smaller advantage, to print fine features with the mask out of focus. However when the techniques are applied using radiation with a narrow band width, as in 13 nm projection lithography, then Fresnel diffraction will cause serious ripples in non-symmetric images.

## Acknowledgments

This work was funded by the National Science and Technology Board and Singapore Ministry of Education under grant RP3979908M. We are grateful for facilities provided by Professor F Cerrina at the University of Wisconsin-Madison.

## References

[1] Vladimirsky Y, Bourdillon A J, Vladimirsky O, Jiang W L and Leonard Q 1999 *J. Phys. D: Appl. Phys.* **32** L114–18

[2] Krasnoperova A A, Rippstein R, Flamholz A, Kratchmer E, Wind S, Brooks C and Lercel M 1999 *Proc. SPIE* **3676** 24–39 (notice that the penumbral blur is about 1 nm, not 5 nm as stated there)

[3] Neureuther A R 1980 Microlithography with soft x-rays *Synchrotron Radiation Research* ed H Winich and S Doniach (New York: Plenum)

[4] Vladimirsky Y 1998 Lithography *Vacuum Ultraviolet Spectroscopy II (Experimental Methods in the Physical Sciences, vol 32)* ed J A Samson and D L Ederer (New York: Academic) ch 10, pp 205–23

[5] Cerrina F 1997 X-ray lithography *Handbook of Microlithography, Micromachining, and Microfabrication* vol 1, ed P Rai-Choudhury (Bellingham, WA: SPIE) ch 3, pp 253–319

[6] Vladimirsky Y 1999 Introduction: limits or limitations *Proc. SPIE* **3676** xvi–xvii

[7] Silverman J 1998 Proximity x-ray lithography: a white paper for the 1998 Sematech Next Generation Lithography Workshop figure 4, Sematech

[8] Ocola L E 1996 Electron–matter interactions in x-ray and electron beam lithography *PhD Thesis* University of Wisconsin-Madison

[9] Fujii K, Tanaka Y, Taguchi T, Yamabe M, Gomei Y and Hisatsugu T 1998 *J. Vac. Sci. Technol.* B **16** 3504–8

[10] Jenkins F A and White H E 1957 *Fundamentals of Optics* (New York: McGraw-Hill)

[11] Bollepalli S B 1999 Image formation in layered structures: with application to x-ray and extreme ultraviolet lithographies *PhD Thesis* University of Wisconsin-Madison

[12] Born M and Wolf E 1986 *Principles of Optics* (Oxford: Pergamon) pp 428–30 and 565–78

[13] Cowley J M 1981 *Diffraction Physics* (Amsterdam: North-Holland)

[14] Van Roey J, Van Der Donk J and Lagasse P E 1981 *J. Opt. Soc. Am.* **71** 803

[15] Bollepalli S B, Khan M and Cerrina F 1998 Modelling image formationin layered structures: application to x-ray lithography *1998 Int. Conf. on Modelling and Simulation of Microsystems, Semiconductors, Sensors and Actuators* (Cambridge, MA:Computational Publications) XV p 53

[16] Kong J R, Leonard Q, Vladimirsky Y and Bourdillon A J 2000 Demagnification-by-bias in proximity x-ray lithography *Proc. SPIE* **3997** at press

[17] Saxton W O, Pitt T J and Horner M 1979 *Ultramicroscopy* **4** 343